ARTICLES
https://doi.org/10.1038/s41594-019-0214-1

nature structural & molecular biology

A symmetric toggle switch explains the onset of random X inactivation in different mammals

Verena Mutzel[1], Ikuhiro Okamoto[2,3], Ilona Dunkel[1], Mitinori Saitou[4,5,6], Luca Giorgetti[7], Edith Heard[8,9] and Edda G. Schulz[1*]

Gene-regulatory networks control the establishment and maintenance of alternative gene-expression states during development. A particular challenge is the acquisition of opposing states by two copies of the same gene, as in the case of the long non-coding RNA *Xist* in mammals at the onset of random X-chromosome inactivation (XCI). The regulatory principles that lead to stable mono-allelic expression of Xist remain unknown. Here, we uncover the minimal regulatory network that can ensure female-specific and mono-alleleic upregulation of Xist, by combining mathematical modeling and experimental validation of central model predictions. We identify a symmetric toggle switch as the basis for random mono-allelic upregulation of Xist, which reproduces data from several mutant, aneuploid and polyploid mouse cell lines with various Xist expression patterns. Moreover, this toggle switch explains the diversity of strategies employed by different species at the onset of XCI. In addition to providing a unifying conceptual framework with which to explore XCI across mammals, our study sets the stage for identifying the molecular mechanisms needed to initiate random XCI.

During developmental cell fate decisions, cells must choose and subsequently maintain alternative transcriptional states. Such a decision-making process occurs at the onset of random X-chromosome inactivation (XCI), where 50% of cells in female embryos will silence the maternal X chromosome (Xm) and 50% the paternal X chromosome (Xp). XCI is initiated during early embryogenesis by mono-allelic upregulation of the long non-coding RNA (lncRNA) Xist (X-inactive-specific transcript) from either the Xp or the Xm, which then induces chromosome-wide gene silencing in *cis*. Xist recruits repressive chromatin modifications, including H3K27me3, to the inactive X, eventually resulting in complete heterochromatinization of the entire chromosome. In this way, mammals ensure dosage compensation for X-linked genes between the sexes[1].

Although all eutherian mammals use Xist to control XCI, they seem to regulate it in different ways[2]. Human and rabbit embryos initially express Xist from both X chromosomes[3], while mice are thought to exhibit strictly mono-allelic expression[4,5]. In rabbits, the bi-allelic phase is very transient, but in human embryos it extends over several days, yet without inducing complete gene silencing[3,6]. Also, some Xist regulators seem to be poorly conserved across species[2]. *Tsix*, the repressive antisense transcription unit of *Xist*, regulates Xist in mice but might not be functional in other mammals[2,7,8], while another lncRNA, XACT, antagonizes Xist in humans[9]. Therefore, different species have been suggested to employ diverse strategies to establish XCI during embryogenesis[2].

To establish the female-specific mono-allelic expression pattern of Xist, a cell must assess the number of X chromosomes, choose one for Xist upregulation, and stabilize two opposing states at the inactive X (Xi), which expresses Xist, and the active X (Xa), where Xist is silent[1]. The underlying regulatory network integrates information on X-chromosomal dosage, since cells with two or more X chromosomes, but not male or XO cells, upregulate Xist[10]. Interestingly, cells with four X chromosomes inactivate three Xs when diploid (X tetrasomy) but only two when tetraploid, suggesting that autosomal ploidy also modulates the onset of XCI[10,11].

As the two *Xist* loci in a cell adopt opposing expression states, important regulatory events must occur in *cis*, on the allele level, indicating a role of X-linked regulators in mediating *cis*-regulation and transmitting X-dosage information. Indeed, several *cis*-acting lncRNA loci function as Xist repressors, like *Tsix* and potentially *Linx*, or as Xist activators, like *Ftx* and *Jpx*[7,12–14]. X-dosage sensing is thought to rely on a *trans*-acting X-linked Xist activator (XA), which by being present at a double dose in female cells, could confer female specificity to XCI[1]. Silencing of XA upon mono-allelic Xist upregulation would reduce its dose and thereby prevent Xist expression from the other allele through a *trans*-acting negative feedback loop[15,16]. Two *trans*-acting Xist activators have been proposed so far, the RNF12 (RLIM) protein, which is silenced by Xist, and the lncRNA Jpx, which escapes XCI[13,15,17].

Several regulators governing the initiation of XCI are known, but their relative contributions and functional interplay, and the underlying regulatory principles remain poorly understood. To rigorously identify the interactions required to initiate random XCI we compare alternative network architectures through mathematical modeling and simulations, and test model predictions experimentally. We show that the cooperation of a *cis*-acting repressor and a *trans*-acting activator is sufficient to ensure female-specific mono-allelic Xist upregulation. They form an extended symmetric toggle switch, which can reproduce the diverse Xist expression patterns in aneuploid and polyploid cells, and in different species. Moreover, we show that in mice, the *cis*-acting repressor identified by our model comparison could be *Tsix*,

[1]Otto Warburg Laboratories, Max Planck Institute for Molecular Genetics, Berlin, Germany. [2]Department of Anatomy and Cell Biology, Graduate School of Medicine, Kyoto University, Kyoto, Japan. [3]Japan Science and Technology (JST), Exploratory Research for Advanced Technology (ERATO), Kyoto, Japan. [4]Institute for the Advanced Study of Human Biology (ASHBi), Kyoto University, Kyoto, Japan. [5]Department of Anatomy and Cell Biology, Graduate School of Medicine, Kyoto University, Kyoto, Japan. [6]Center for iPS Cell Research and Application (CiRA), Kyoto University, Kyoto, Japan. [7]Friedrich Miescher Institute for Biomedical Research, Basel, Switzerland. [8]Institut Curie, PSL Research University, CNRS UMR3215, INSERM U934, Paris, France. [9]European Molecular Biology Laboratory (EMBL), Directors' research unit, Heidelberg, Germany. *e-mail: edda.schulz@molgen.mpg.de

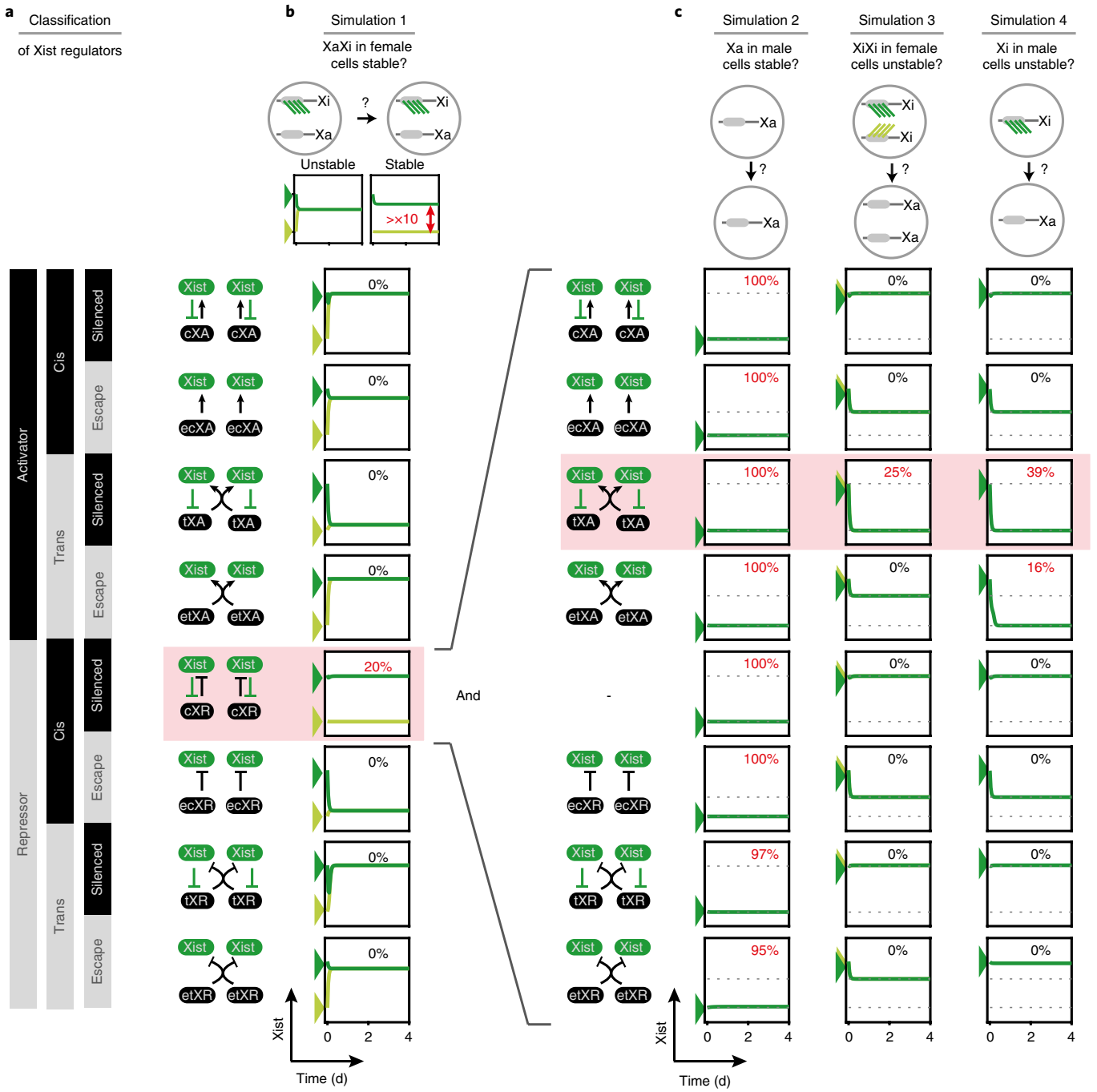

Fig. 1 | Comparison of alternative model structures. a, Classification of X-linked Xist regulators, depending on whether they act as activators (XA) or repressors (XR), whether they act in *cis* (c) or in *trans* (t), and whether they are silenced during XCI or escape (e). Right, schematic depiction of the networks formed by Xist and each regulator. **b**, Each network was translated into a mathematical model (ODE), describing two X chromosomes, each carrying *Xist* and the respective regulator. Each model was simulated with >10,000 randomly chosen parameter sets initiating from an XaXi state (schematic, top), where Xist is expressed from one chromosome (dark green) and not from the other (light green). One example simulation is shown for each network, and the percentage of tested parameter sets where the XaXi state was stably maintained is indicated (in red if >0%). **c**, The *cis*-acting repressor (cXR), which could maintain the XaXi state in **b**, was combined with all other regulator classes to build seven more complex models. For all parameter sets that could maintain the XaXi state, three additional simulations were performed to test whether the $Xist^{OFF}$ state (Xa) was maintained in male cells with a single X (simulation 2), whether bi-allelic Xist expression (XiXi) would be unstable in female cells (simulation 3) and whether Xist expression from the single X (Xi) in male cells would be unstable (simulation 4). One example simulation is shown for each model and the percentage of parameter sets that fulfil these criteria are shown. Dotted lines indicate the Xa and Xi state from the simulation in **b** and arrowheads denote the initial conditions. Shaded boxes indicate the model that can reproduce the experimental observations.

the antisense transcript of *Xist*. Our systems biology approach has thus identified the regulatory principles governing the onset of XCI and provides a unifying framework for Xist regulation across species.

Results

A core network that can maintain mono-allelic Xist expression. To investigate the regulatory principles governing mono-allelic and

female-specific Xist expression, we systematically screened alternative architectures of the underlying regulatory network. X-linked Xist regulators were sorted into eight categories depending on whether they activate (A) or repress (R) Xist, whether they act in *cis* (c) on the same chromosome or in *trans* (t) on both chromosomes and whether they are silenced during XCI or escape (e) (Fig. 1a). Using ordinary differential equations (ODEs), we built eight mathematical models of a cell with two Xs containing Xist and one regulator type (see Supplementary Note 1).

To understand which networks can maintain mono-allelic Xist expression, each model was simulated starting from an XaXi state, where Xist is only expressed from the Xi (simulation 1, Fig. 1b). Each simulation was performed for more than 10,000 randomly chosen parameter sets, combining different transcription rates and activation or repression strengths, to test whether a given network could in principle reproduce the experimental behavior. Only the network with a *cis*-acting Xist repressor (cXR) was able to maintain mono-allelic Xist expression (in 20% of parameter combinations, Fig. 1b). We further tested another 28 models, each combining two regulator types instead of one. Again, only the seven cXR-containing models could stabilize mono-allelic expression, showing that cXR is the only factor strictly required to maintain the XaXi state (see Supplementary Note 1).

Next, we examined which network could also prevent Xist upregulation from the single X in male cells (simulations 2 + 4) and from both Xs in female cells (simulation 3), by initiating the simulations from an Xa, XiXi or Xi state, respectively (Fig. 1c). We tested all eight models that maintained the mono-allelic state in simulation 1, which contained cXR either alone or in combination with another regulator type. All tested networks maintained the Xa state in simulation 2, but a *trans*-acting Xist activator (tXA) was required to prevent erroneous Xist expression in simulations 3 and 4. Female specificity of Xist upregulation does not require tXA to be subject to XCI (simulation 4); however, to prevent bi-allelic expression tXA must be silenced (simulation 3). A comprehensive screening of 36 alternative network architectures thus identified a single minimal network (cXR-tXA) that can ensure the correct Xist expression pattern (Fig. 2a). Although the *trans*-activator hypothesis has been proposed previously[15], we show that correct XCI also requires a *cis*-acting repressor.

The cXR–tXA model explains Xist patterns in diploid, polyploid and polysomic cells. We then asked whether the identified network could also recapitulate the initial establishment of a mono-allelic state (Fig. 2a,b). The XaXa-to-XaXi transition, where Xist is randomly upregulated from either the Xm or Xp, cannot be simulated in the deterministic ODE framework used above. We therefore developed a stochastic cXR–tXA model that simulates individual cells and accounts for random fluctuations (see Supplementary Note 2). For a subset of parameter values, the network could indeed

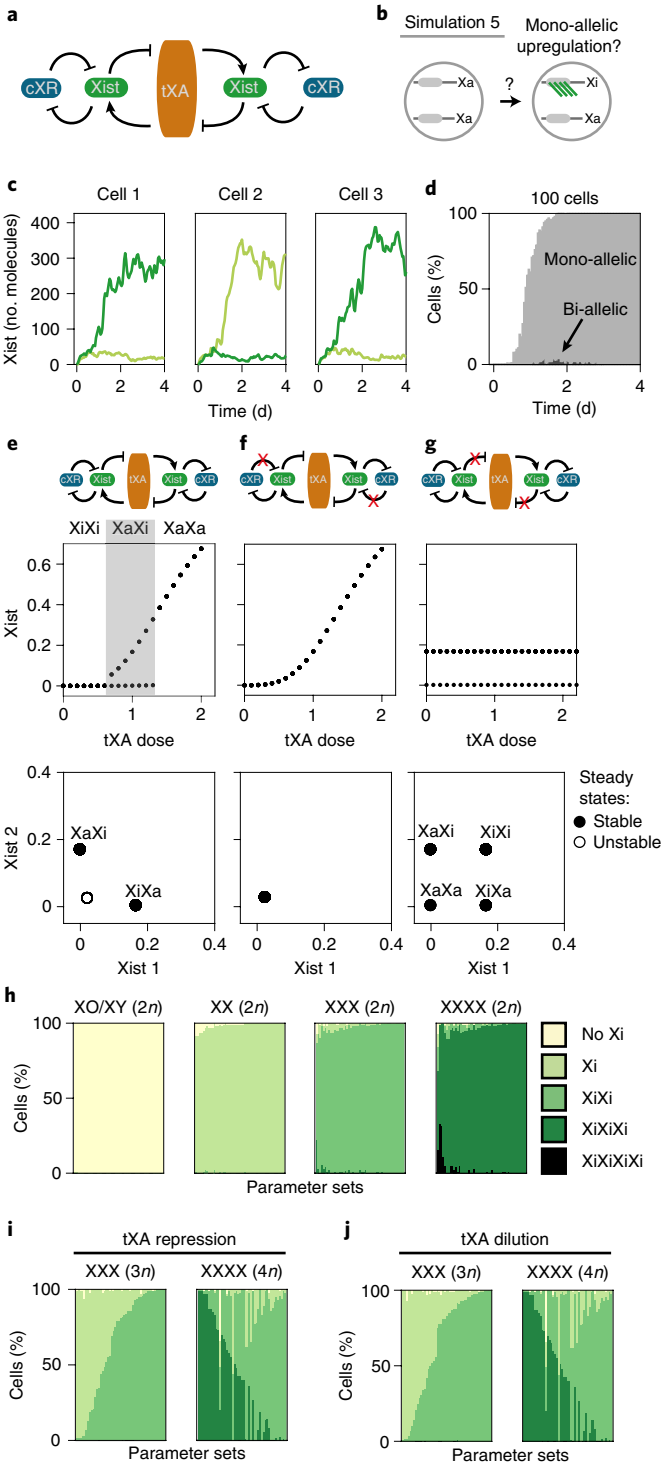

Fig. 2 | The cXR–tXA model can recapitulate Xist patterns in male, female, aneuploid and polyploid cell lines. a,**b**, Schematic representation of the cXR–tXA model (**a**) and of the stochastic simulation (**b**) shown in **c** and **d**, which starts from the XaXa state found in undifferentiated cells. **c**,**d**, Simulation of Xist upregulation for one example parameter set, showing three individual cells (**c**) and a population of 100 cells (**d**). Light and dark green in **c** represent Xist levels expressed from the two X chromosomes; light and dark grey in **d** represent mono- and bi-allelic Xist expression, as indicated. **e**–**g**, Steady-state Xist levels simulated deterministically (as in Fig. 1b) either for the full cXR–tXA model (**e**) or in the absence of either cXR-mediated repression (**f**) or tXA-mediated activation (**g**). Allelic (top) and cellular (bottom) steady-state levels are shown. Shaded area in **e** indicates the bistable regime for a single tXA dose corresponding to the mono-allelic XaXi state. Filled and open circles indicate stable and unstable steady states, respectively. In **g**, tXA was assumed to be present at a constant single tXA dose (1× tXA). **h**, Simulations of diploid cells with either one (left, male), two (middle left, female), three (middle right, X trisomy) or four X chromosomes (right, X tetrasomy). Stacked bar graphs show the classification of Xist patterns in simulations with 50 parameter sets that can generate robust mono-allelic Xist upregulation in female diploid cells. **i**–**j**, Stacked bar graphs show the classification of Xist patterns in simulations of triploid (left) and tetraploid cells (right) assuming that tXA is repressed by autosomal factors in a dose-dependent manner (**i**) or that tXA is diluted 1.5- and 2-fold in tri- and tetraploid cells, respectively, due to increased nuclear volume in polyploid cells (**j**). Details on the simulations are given in Supplementary Note 2.

simulate robust mono-allelic Xist upregulation (example simulations in Fig. 2c,d; for detailed analysis see Supplementary Note 2) and even reproduce experimental measurements quantitatively (Supplementary Fig. 1a).

To understand how the cXR–tXA model controls mono-allelic Xist upregulation, we analyzed the expression states of Xist at the allele (Fig. 2e, top) and at the cell level (Fig. 2e, bottom). In post-XCI cells (XaXi), when one tXA copy is silenced (tXA dose = 1), each allele can maintain either low or high Xist expression (bistability), corresponding to the Xa and Xi, respectively (Fig. 2e, top). Before XCI (tXA dose = 2) only the high Xist expression (Xist-high) state exists, resulting in female-specific Xist upregulation (XaXa, Fig. 2e). Upon complete tXA silencing in the XiXi state, Xist expression cannot be sustained because the Xist-high state becomes unstable (XiXi, Fig. 2e). Consequently, the mono-allelic states (XaXi and XiXa) but not the Xist-negative and bi-allelic states, are stable at the cell level (Fig. 2e, bottom). Allelic and cellular bistability require both regulators. Without cXR only a single allelic state remains (Fig. 2f), whereas in the absence of tXA additional global states appear, such that coordination of the two *Xist* loci is lost and both the XaXa and XiXi states become stable (Fig. 2g). In conclusion, this bistable behavior is generated by mutual repression of Xist and cXR, which form a *cis*-acting double-negative (therefore positive) feedback loop. tXA, which mediates a second, *trans*-acting feedback ensures female-specific and mutually exclusive expression of the two *Xist* alleles.

For further validation, we tested whether the cXR–tXA model could reproduce the phenotype of X aneuploidies, which inactivate all Xs except one[10]. Nearly all parameter sets that can reproduce mono-allelic Xist upregulation in diploid female cells correctly predict no Xist expression in male and XO cells and bi- and tri-allelic expression in X-chromosome trisomies and tetrasomies, respectively (Fig. 2h). Although diploid (2n) cells with four Xs inactivate three of them, tetraploid (4n) cells that also have four Xs only inactivate two[11]. Similarly, X-trisomic diploid cells inactivate two Xs, while triploid cells (3n) are a mixture of cells with one and two Xi[11,18]. We simulated polyploidy in two ways, assuming either that autosomal factors would repress tXA or that an additional copy of the genome leads to a 50% increase in nuclear volume[19], thus resulting in an effective tXA dilution (see Supplementary Note 2 for details). In both scenarios, the effective tXA concentration would be similar in diploid and in tetraploid nuclei. The majority of parameter sets that can reproduce mono-allelic Xist upregulation in diploid XX cells correctly predicted a mixture of cells in the Xi and XiXi states in triploid, and the XiXi state in tetraploid cells in both scenarios (Fig. 2i, j). Parameter sets that can reproduce mono-allelic Xist upregulation in diploid female cells thus also correctly reproduce the different XCI patterns in X tri- and tetrasomies and in tri- and tetraploidies.

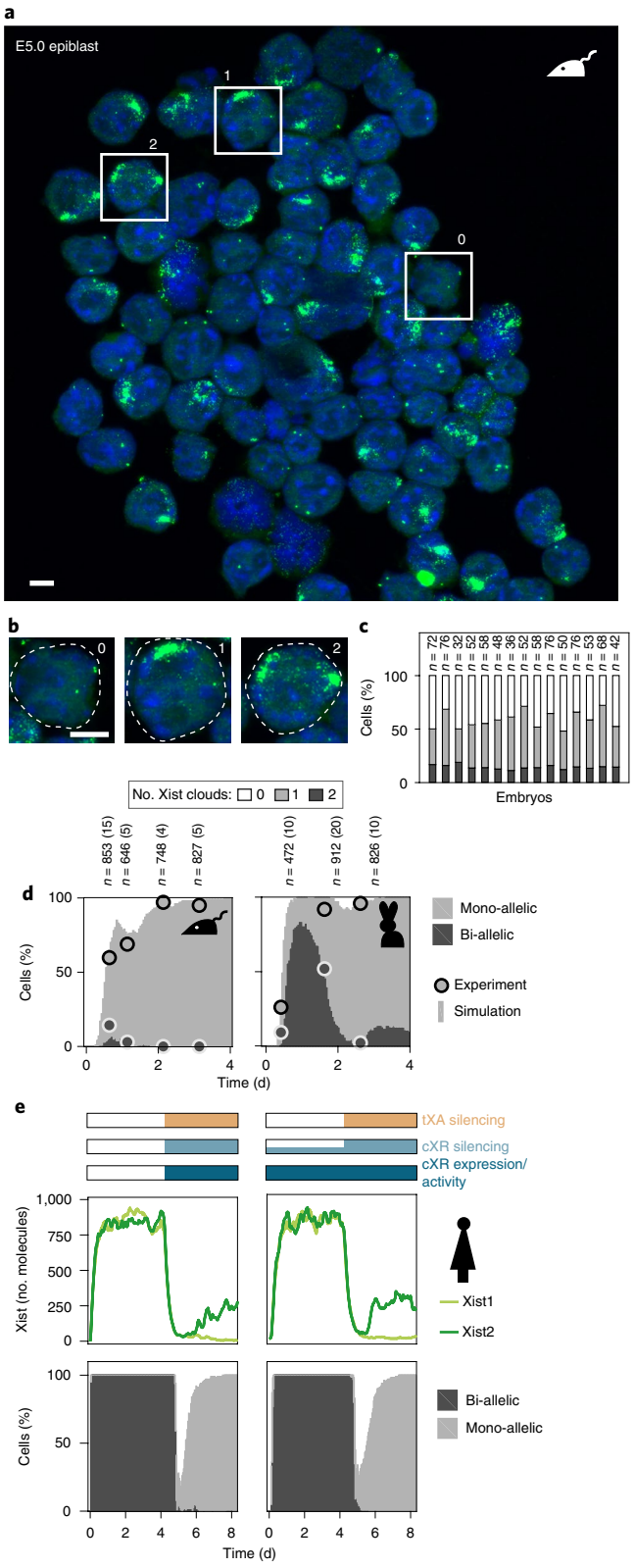

Fig. 3 | The cXR–tXA model reproduces transient bi-allelic expression in different species. a–c, Non strand-specific RNA FISH (green) to detect both Xist and Tsix, and nuclear staining (blue) of female mouse epiblast cells at E5.0 of embryogenesis. Scale bar, 5 µm. **b**, Example cells with 0, 1 and 2 Xist clouds marked in **a** are enlarged, dashed white lines indicate the outlines of the nuclei. **c**, The percentage of cells in each category is given across 15 female embryos, the number of cells counted is given above each bar. **d**, Fraction of cells exhibiting mono-allelic (light grey) and bi-allelic Xist expression (dark grey) during early mouse (left) and rabbit development (right). Experimental data (circles) are shown together with a simulation using the parameter set that best explains the data. The experimental data are taken from refs. [3,51] and **a–c**. The total number of cells (*n*) counted for each time point is given on top, together with the number of embryos from which the data was pooled (in parentheses). **e**, Simulation of bi-allelic expression upon reduced Xist-mediated silencing as observed in human embryos, assuming that in the first 4 d of the simulation either silencing (orange and light blue bars) and cXR expression (dark blue) is absent (left) or that cXR is silenced partially (light blue), while tXA (orange) is unaffected by Xist (right), as indicated. Simulations of an individual cell (top) and a population of 100 cells (bottom) for one example parameter set are shown. A summary of all parameter sets is given in Supplementary Fig. 2b. Source data for **c** and **d** are available online.

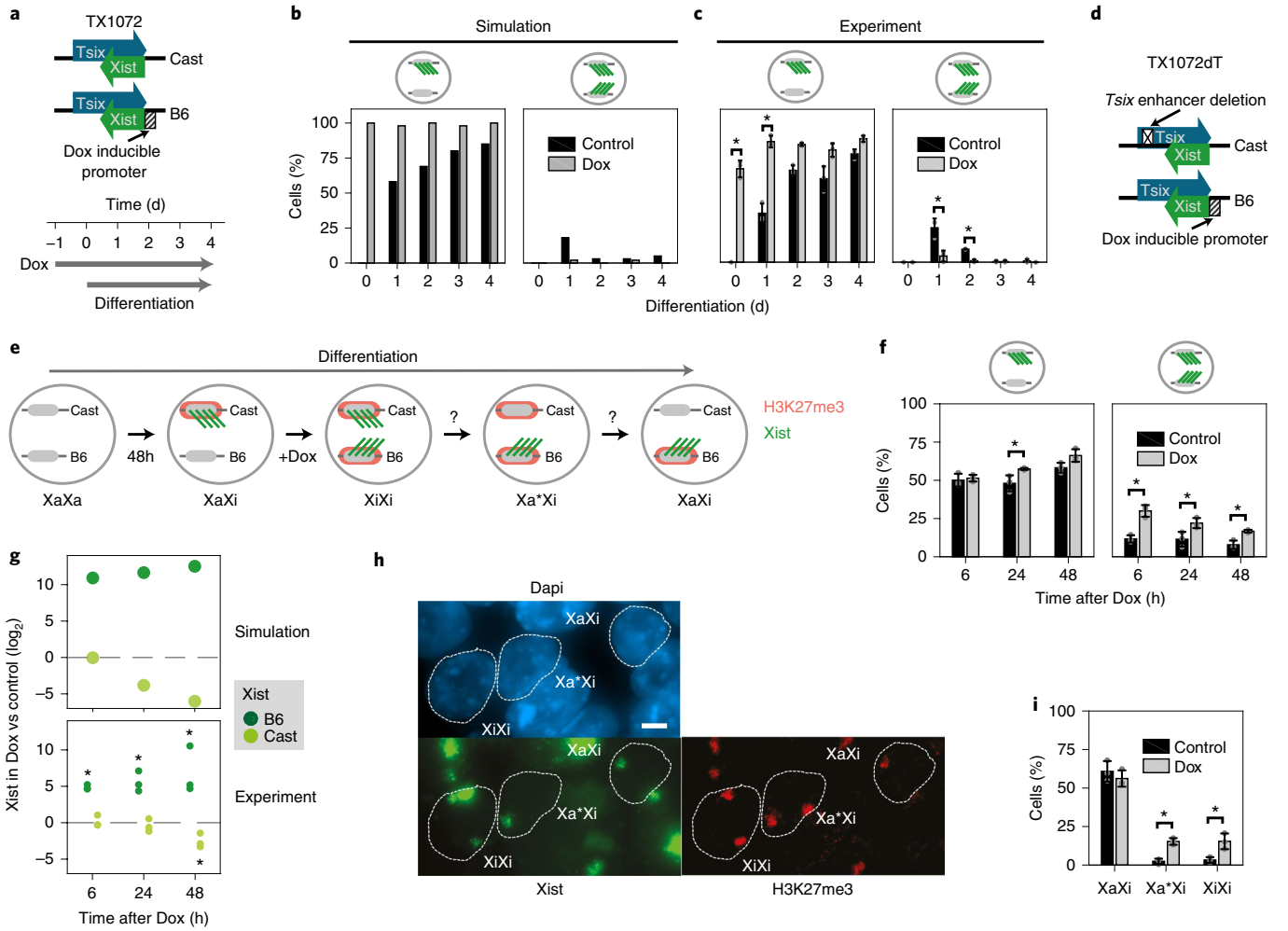

Fig. 4 | Bi-allelic Xist upregulation is reversible. a, Schematic representation of the cell line used (top) and treatment performed (bottom) in **b** and **c**. **b**,**c**, In a simulation (**b**) and in an experiment (**c**), cells were treated with doxycycline 1 d before differentiation. The percentage of cells showing mono-allelic (left) and bi-allelic Xist upregulation (right) is shown. **b**, The simulation for one example parameter set is shown; the results for all tested parameter sets can be found in Supplementary Fig. 3a. **c**, Xist patterns were assessed by RNA FISH. Mean and s.d. of $n = 3$ independent experiments are shown (>80 cells per replicate, for details see source data). **d**–**i**, Bi-allelic Xist upregulation is artificially induced by treating TX1072dT cells (**d**) with doxycycline after 48 h of differentiation. The model predicts Xist downregulation from the Cast chromosome, potentially with a transition through an Xa* state, where H3K27me3 (red) is still enriched while Xist (green) has already been downregulated (**e**). Xist expression pattern at different time points after doxycycline addition, as assessed by RNA FISH, is also shown (**f**). Mean and s.d. of $n = 3$ independent experiments are shown (>100 cells per replicate, for details see source data). In **g**, Xist expression levels from the B6 and Cast alleles are shown at different time points after doxycycline treatment, as predicted by the simulation (top) and measured experimentally by allele-specific amplicon sequencing (bottom). In the simulation, one example parameter set is shown; results for all other tested parameter sets can be found in Supplementary Fig. 3b. Immunofluorescence followed by RNA FISH was used to detect Xist and H3K27me3 48 h after doxycycline induction (**h**,**i**). Three states were quantified (XaXi, Xa*Xi, XiXi), as shown in the example image (**i**). Scale bar, 5 µm. Mean and s.d. of $n = 3$ independent experiments are shown (>120 cells per replicate). *$P < 0.05$ in two-sample (**c**,**f**,**i**) or one-sample (**g**) two-sided *t*-test. Source data for **b**,**c**,**f**,**g**,**i** are available online.

The cXR–tXA model explains Xist patterns in different species. In the cXR–tXA model, bi-allelic Xist upregulation can be reversed through tXA silencing (Fig. 2e). This could be the mechanism that resolves transient bi-allelic expression during rabbit embryogenesis[3]. Interestingly, bi-allelic Xist expression has not been observed in mouse embryos, but can occur in differentiating mouse embryonic stem cells (mESCs) (for example Supplementary Fig. 1a, dots)[20]. To test whether initiation of random XCI is also associated with bi-allelic Xist upregulation *in vivo*, we assessed the Xist expression pattern using RNA FISH (fluorescence in situ hybridization) in the embryonic day 5 (E5.0) epiblast, where random XCI is first initiated, and observed 15–20% of cells with two Xist clouds (Fig. 3a–c). In agreement with a recent study[21], we conclude that transient bi-allelic Xist expression occurs during mouse development, but less frequently than in rabbits or humans.

Our cXR–tXA model can generate different degrees of transient bi-allelic expression, depending on the relative time scales of tXA silencing and Xist upregulation (Supplementary Fig. 2a). A single network architecture can thus reproduce experimental data from both mouse and rabbit embryos, just assuming different values for the reaction rates (Fig. 3d). In contrast to bi-allelic Xist expression in rabbits, that in human embryos persists over several days without inducing gene silencing (only dampening of gene expression)[3,6]. How bi-allelic expression is resolved is unknown because this happens only after implantation into the uterus. In the cXR–tXA model, reduced gene silencing would lead to bi-allelic Xist expression, if (1)

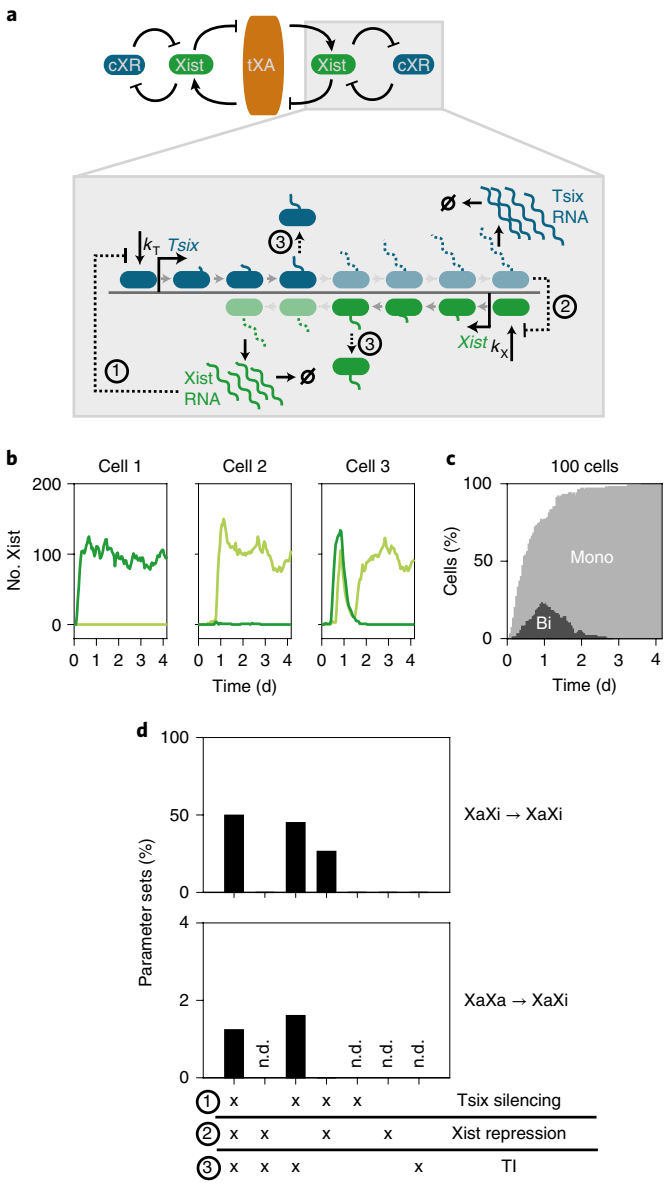

Fig. 5 | Predicted *cis*-acting feedback can be mediated by antisense transcription. a, Schematic representation of the model in which *Tsix* acts as the predicted *cis*-acting repressor: RNA Pol II complexes can bind to the *Tsix* (blue) and *Xist* (green) promoters and then move along the gene in a convergent fashion. Mutual repression occurs at three levels: (1) silencing of the *Tsix* promoter by Xist RNA, (2) repression of the *Xist* promoter by antisense transcription, and (3) random removal of one Pol II complex, if two antisense Pol II complexes occupy the same DNA element. Black dotted lines indicate interactions removed in the reduced models in **d**. Lighter colors and dotted nascent RNA indicate potential interruption of transcription through TI. **b**,**c**, Stochastic simulation of Xist upregulation for one example parameter set for the model shown in **a**, showing three individual cells (**b**) and a population of 100 cells (**c**). Light and dark green in **b** represent Xist levels expressed from the two X chromosomes, light and dark grey in **c** represent mono- and bi-allelic Xist expression, as indicated. **d**, Testing of model simplifications for the network in **a**, where *Xist* and *Tsix* interact through one or two of the three repressive mechanisms, as indicated. The percentage of parameter sets that can maintain the XaXi state (top) and that can initiate mono-allelic Xist upregulation (bottom) in a stochastic simulation for each model are shown. Mono-allelic upregulation was only tested for parameter sets that could maintain the XaXi state (others not determined (n.d.)). Source data for **d** are available online.

cXR is not yet expressed (Fig. 3e and Supplementary Fig. 2b, left) or if (2) cXR would be partially silenced ('dampened', Fig. 3e and Supplementary Fig. 2b, right), while tXA completely resisted Xist-mediated silencing, assuming variable susceptibility to dampening across genes. The onset of complete silencing (together with cXR upregulation in scenario (1)) would then induce the transition to the mono-allelic state. In summary, the cXR–tXA model can reproduce the different degrees of transient bi-allelic expression observed across mammals.

Bi-allelic Xist upregulation is reversible. To validate the model experimentally, we tested its prediction that accelerating Xist upregulation on one allele (increased time before switching ON of the other allele) should reduce the extent of transient bi-allelic Xist expression (Supplementary Fig. 2a). We used an mESC line (TX1072) that was derived from a cross between two polymorphic mouse strains (C57BL6/J × Cast/EiJ), referred to herein as B6 and Cast, respectively, and that carries a doxycycline-inducible promoter upstream of *Xist* on the B6 X chromosome (Fig. 4a, top), such that Xist upregulation is accelerated by doxycycline treatment[22]. When cultured in 2i medium, the cells undergo random XCI upon differentiation, frequently passing through a phase of bi-allelic Xist upregulation[20]. As predicted (Fig. 4b), doxycycline addition 1 d before differentiation reduced bi-allelic Xist upregulation from approximately 25% to less than 5% of cells (Fig. 4c). Accelerating Xist upregulation can therefore modulate the extent of bi-allelic Xist expression.

Another prediction that we aimed to test was that transient bi-allelic expression could be resolved to a mono-allelic state (see previous section). To this end, we artificially increased bi-allelic upregulation and assessed the system's response. We deleted the *DXPas34* enhancer of *Tsix* from the Cast X chromosome in TX1072 mESCs (Fig. 4d), which results in preferential Xist upregulation from that chromosome[7]. After 48 h of differentiation, *Xist* was induced by doxycycline also from the other allele (B6) (Fig. 4e), thus increasing the amount of bi-allelically expressing cells from 12% to 30% (Fig. 4f). As Xist expression from the B6 chromosome is maintained by doxycycline, the cells are predicted to downregulate Xist from the Cast chromosome to resolve the bi-allelic expression state (Fig. 4g top, light green). Xist expression was quantified in an allele-specific way through amplicon sequencing of single-nucleotide polymorphisms (SNPs) on cDNA. As predicted, Xist from the Cast chromosome was significantly downregulated 48 h after doxycycline treatment compared to the untreated control (Fig. 4g, bottom, light green).

To distinguish whether Xist upregulation had indeed been reversed or whether silencing of both Xs had only led to cell death, we performed two additional experiments. To assess viability, we quantified EdU incorporation during replication and found only slightly less EdU-positive cells in bi-allelic compared to mono-allelic cells after 24 h of doxycycline treatment (88% vs 94%, Supplementary Fig. 3c,d). Therefore, cell death only has a minor role in the transition from the bi-allelic to the mono-allelic state. We also performed RNA FISH with immunofluorescence (immuno-RNA FISH) for Xist and H3K27me3, which is recruited to the chromosome following Xist RNA coating[1]. After 48 h of doxycycline treatment we identified chromosomes that had ceased to express Xist but were still enriched for H3K27me3 (as this mark is lost more slowly from the X chromatin), and named these Xa* (schematic in Fig. 4e and example image Fig. 4h). Cells that had reverted from a bi-allelic to a mono-allelic state (Xa*Xi) were rarely observed after 4 d of differentiation without doxycycline (<5%), but constituted more than 10% of cells upon bi-allelic Xist induction (Fig. 4i). In conclusion, bi-allelic Xist expression can indeed be resolved by downregulation of one *Xist* allele.

A mechanistic cXR–tXA model of murine Xist regulation. The identification of the regulator classes required for mono-allelic Xist upregulation paves the way to uncovering the molecular identities of cXR and tXA. For the tXA factor, no candidate with all required characteristics has been identified (see discussion for details). Among known cXRs, the repressive antisense transcript of *Xist, Tsix*, is a well characterized *cis* repressor and has been suggested previously to function as a switch to establish mono-allelic Xist expression[23]. Mutual inhibition between *Xist* and *Tsix* could thus form the *cis*-acting double negative feedback loop that we have predicted to generate bistability[24]. To test whether antisense transcription-mediated repression could generate bistability in *cis*, we developed a mechanistic model of the *Xist–Tsix* locus, describing transcriptional initiation, RNA polymerase II (Pol II) elongation and RNA degradation of this antisense gene pair (Fig. 5a, for details see Supplementary Note 3). The model assumes three mechanisms for mutual repression of *Xist* and *Tsix*: (1) Xist RNA-dependent silencing of the *Tsix* promoter, (2) *Tsix*-transcription dependent repression of the *Xist* promoter, and (3) transcriptional interference[25], occurring when Pol II complexes transcribing opposite strands meet, as modeled in several previous studies[26,27]. As two Pol II complexes probably cannot bypass each other[28], we assumed that one complex will be removed from the locus. Through a multi-step simulation process, we identified parameter sets that reproduced random mono-allelic Xist upregulation (example in Fig. 5b,c). This specific behavior is expected to occur only in a precise parameter regime and is therefore observed for a small fraction (~1%) of all tested parameter sets for such a complex model (seven parameters). To understand which inhibitory mechanisms were actually required, we tested six reductions of the full model ([1,2,3]). Although two of the reduced models ([1,2], [1,3]) were able to maintain the XaXi state, only one of them [1,3], which retained Xist-dependent silencing and transcriptional interference, could reproduce mono-allelic Xist upregulation (Fig. 5d). We named the [1,3] model the 'antisense model' and used it for all further simulations. Interestingly, the reduced model [1,2], which lacked transcriptional interference, could maintain but not establish the XaXi state (compare Fig. 5d top vs bottom), because the transition between the regime of stable XaXi maintenance and Xist upregulation was too gradual (Supplementary Fig. 4). A twofold change in tXA levels did not allow a robust transition between the regimes, suggesting that transcriptional interference might have an important role at the *Xist–Tsix* locus.

Transcriptional interference at the *Xist–Tsix* locus. To validate the existence of transcriptional interference at the *Xist–Tsix* locus experimentally, we assessed whether forced *Xist* transcription would interfere with *Tsix* elongation. We used several mESC lines carrying the TX allele, in which the endogenous *Xist* gene can be controlled by doxycycline (Fig. 6a), thus uncoupling Xist regulation from *Tsix* activity. Upon *Xist* induction in female TX1072 cells and an XO subclone of that line[22] we quantified Tsix RNA transcribed from the TX allele by allele-specific analysis through pyrosequencing and by qPCR, respectively (primer positions in Fig. 6b). In both cell lines, Tsix upstream of the overlapping region (5′) was barely

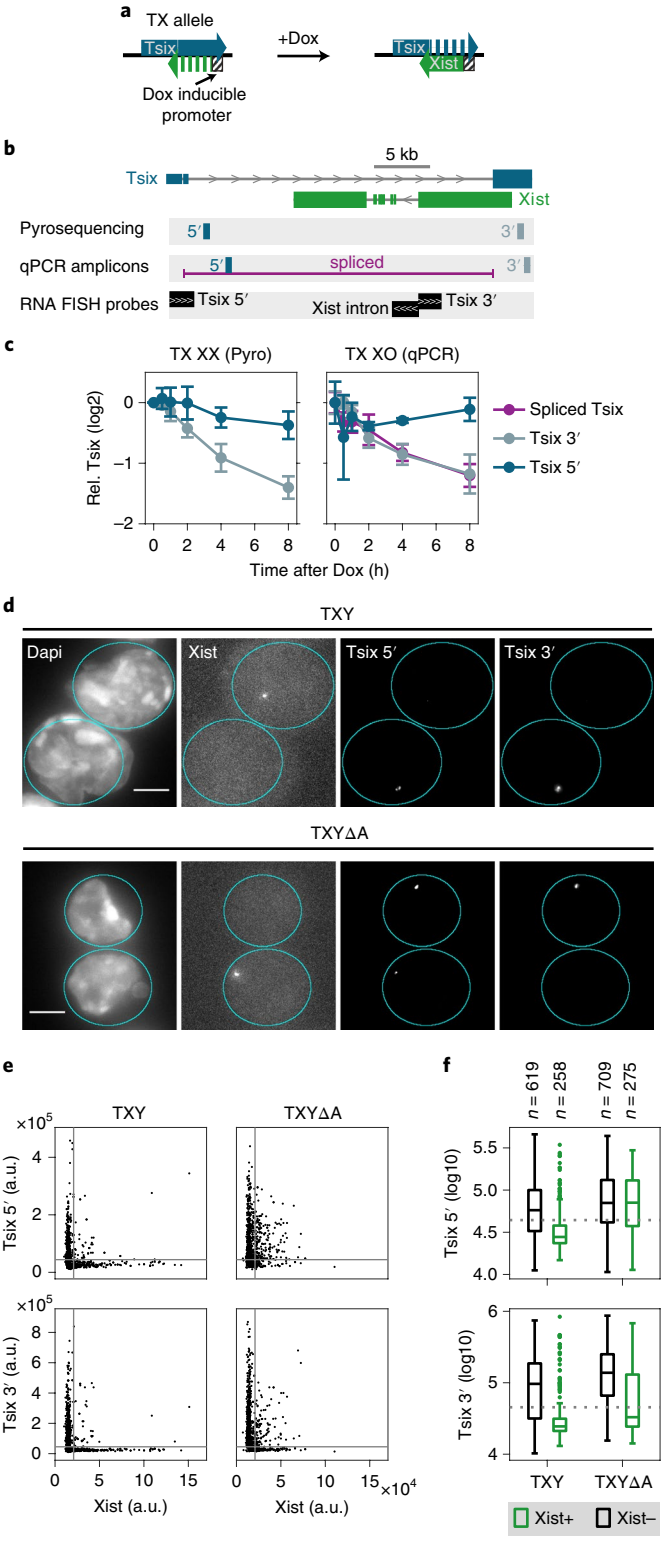

Fig. 6 | Transcriptional interferences at the *Xist–Tsix* locus. a, The TX allele carries a doxycycline-inducible promoter driving the endogenous *Xist* gene and was used to investigate whether *Xist* transcription would interfere with *Tsix* elongation (in **c**–**f**). **b**, Position of primers and probes used in **c**–**f**. **c**, TX1072 XX (left) and TX1072 XO ESCs (right) were treated with doxycycline for 8 h and *Tsix* transcription from the TX allele was assessed by pyrosequencing (XX) or qPCR (XO) at different positions within the *Tsix* gene. Mean and s.d. of $n=3$ independent experiments are shown. **d**–**f**, TXY and TXYΔA ESCs were treated with doxycycline for 24 h and nascent transcription of *Xist* and *Tsix* (5′ and 3′) was assessed by RNA FISH (probe positions in **b**). Example images (**d**) and quantification (**e**) of $n=877$ (TXY) and $n=984$ cells (TXY ΔA) are shown; each dot represents the measured signal intensities of a single allele. Scale bar, 5 µm. Grey lines indicate the detection threshold estimated from negative control regions. Box plots of *Tsix* signal intensity (**f**) at *Xist*+ (green) and *Xist*− alleles (black) in the two cell lines as indicated (center line, median; box limits, upper and lower quartiles; whiskers, most extreme data points not considered outliers; points, outliers). The data shown in **e**,**f** were pooled from 3 independent biological replicates (individual replicates are shown in Supplementary Fig. 5). Source data for **c**,**e**,**f** are available online.

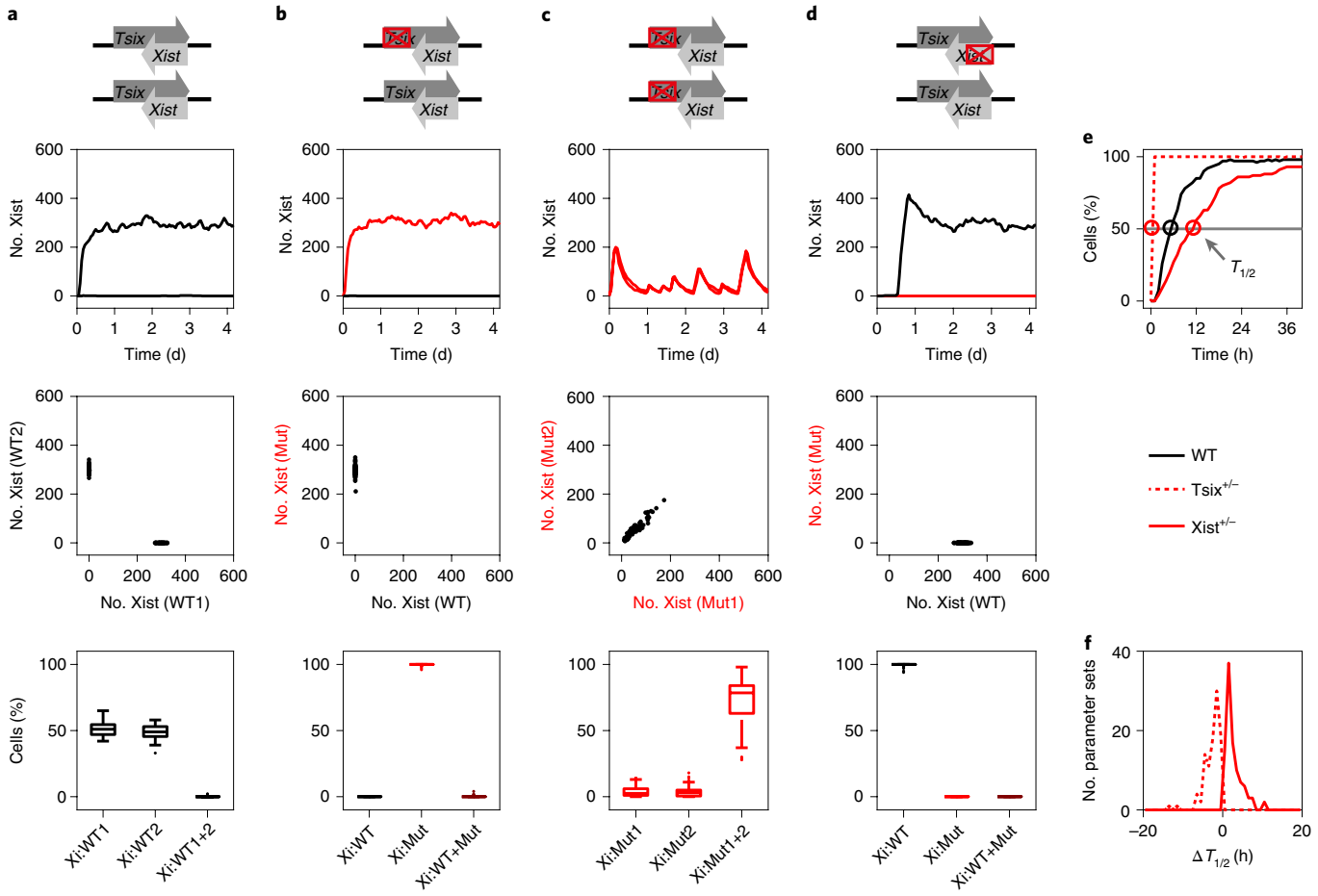

Fig. 7 | Simulation of *Xist* and *Tsix* mutant cell lines. a–d Simulations of *Xist* and *Tsix* mutant cell lines as indicated on top. Representative simulation of Xist levels produced by the wild-type (WT, black) and mutant (Mut, red) chromosomes in a single cell (upper middle) and by 100 cells (lower middle). Boxplots (bottom) show the percentage of cells expressing Xist mono-allelically from wild-type or mutant X or bi-allelically for $n=100$ simulated parameter sets (center line, median; box limits, upper and lower quartiles; whiskers, most extreme data points not considered outliers; points, outliers). **e**,**f** Xist upregulation is accelerated in *Tsix*$^{+/-}$ cells and delayed in *Xist*$^{+/-}$ cells. A representative simulation (**e**) and the distribution of the change of half time ($\Delta T_{1/2}$) in the mutant genotypes (**f**) are shown.

affected by *Xist* induction (Fig. 6c, dark blue), while quantification downstream of *Xist* (3′) revealed a reduction by approximately 50% after 8 h of doxycycline treatment (Fig. 6c, light blue). Spliced Tsix was also strongly reduced, as the splice acceptor site is close to the 3′ end (Fig. 6c, purple). These results suggest that *Xist* induction interferes with *Tsix* elongation.

To further validate transcriptional interference at the *Xist*–*Tsix* locus, we measured nascent transcription by quantitative microscopy at the single-cell level through RNA FISH with intronic oligonucleotide-based probes in a male TX mESC line (TXY)[29]. For *Tsix*, we designed two different probes to detect transcription upstream of *Xist* (5′) and within the overlapping region (3′) (Fig. 6b). As expected, transcription of *Xist* and *Tsix* was mutually exclusive in nearly all cells after 1 d of doxycycline treatment (Fig. 6d,e, left). To be able to observe transcriptional interference independent of Xist RNA-mediated silencing, we used the silencing-deficient TXYΔA line carrying a deletion of the *Xist* A repeat[29]. In this line, mutually exclusive detection of *Xist* and *Tsix* in the overlapping region was still observed, while the *Tsix* 5′ signal was now largely unaffected by *Xist* (Fig. 6e, right). When comparing the signal intensity of the two *Tsix* probes at *Xist* transcribing (*Xist*+) and not transcribing (*Xist*–) alleles, both *Tsix* signals were strongly reduced on the *Xist*+ alleles in the TXY line, probably owing to Xist RNA-mediated silencing of *Tsix*. In TXYΔA cells, the *Tsix*-5′ region was unaffected by *Xist*, but the 3′ position was strongly reduced, albeit to a lesser extent than in TXY cells (Fig. 6f). Although wild-type *Xist* induces an even more complete repression, transcriptional interference clearly perturbs transcriptional elongation at the *Xist*–*Tsix* locus, thus validating a central assumption of the antisense model.

***Xist* and *Tsix* mutant phenotypes.** To further validate the antisense model, we simulated known *Xist* and *Tsix* mutant phenotypes. For 100 parameter sets that could reproduce mono-allelic Xist upregulation four genotypes were simulated: wild-type, *Tsix*$^{+/-}$, *Tsix*$^{-/-}$ and *Xist*$^{+/-}$ (Fig. 7a–d). In our simulations, XCI in wild-type cells is random, such that 50% of cells that will express Xist from one or the other X (Fig. 7a, bottom). In agreement with experimental observations[7,30], heterozygous *Tsix* and *Xist* mutants undergo non-random XCI, where the mutant and wild-type Xs are silenced in *Tsix*$^{+/-}$ and *Xist*$^{+/-}$ cells, respectively (Fig. 7b,d, bottom). For homozygous *Tsix* mutants, ‘chaotic’ XCI has been described with a mixture of cells inactivating one or two X chromosomes[31]. In our simulations we observe Xist oscillations in this mutant, where bi-allelic Xist upregulation results in complete tXA silencing and subsequent Xist downregulation, followed by another round of bi-allelic upregulation (Fig. 7c, top). In agreement with the experimental phenotype, these simulations show a high frequency of bi-allelic Xist expression (Fig. 7c, bottom). We also analyzed the kinetics of Xist upregulation,

Table 1 | X-linked Xist regulators

Regulator class	Putative members
cXA	–
ecXA	*Ftx*[14], *Jpx*[13,17,52]
tXA	RNF12 (refs. [15,37,41])
etXA	*Jpx*[13,17]
cXR	*Tsix*[7], *Linx*[12]
ecXR	–
tXR	–
etXR	–

because XCI has been found to be accelerated in *Tsix*$^{+/-}$ cells, but slowed down in *Xist*$^{+/-}$ mESCs[16]. We calculated the half time of Xist upregulation ($T_{1/2}$), at which 50% of cells would have turned on *Xist* (example in Fig. 7e), and compared this value between mutant and wild-type simulations. For all parameter sets tested, a *Tsix* mutation indeed reduced and an *Xist* mutation increased the half time of Xist upregulation (Fig. 7f). These results support antisense-mediated repression of *Tsix* as a promising candidate mechanism for the predicted bistable feedback loop in mice.

Discussion

Through screening 36 alternative network architectures, we have identified a core network that can recapitulate random mono-allelic and female-specific Xist upregulation. This network, consisting of a *trans*-acting activator and a *cis*-acting repressor, resembles an 'extended toggle-switch', which is thought to govern many cell fate decisions by generating mutually exclusive expression of antagonizing lineage-specifying factors[32]. Two transcription factors, such as PU.1 and Gata1 (driving myeloid and lymphoid differentiation, respectively), mutually repress each other in a classical toggle switch[32], whereas the two *Xist* alleles inhibit each other through silencing of the *trans*-activating tXA factor. However, this inhibition cannot be directional, as reduction of any *trans*-acting regulator affects both *Xist* loci. Our analysis shows that the establishment of two alternative states in such a symmetric network requires a local positive feedback mediated by a *cis*-repressor, cXR, to memorize the initial choice of the inactive X, at least until the two states are locked in by epigenetic mechanisms such as DNA methylation[1]. As transcription factors that drive cell fate decisions often promote their own expression through similar positive feedback regulation, cells seem to employ similar regulatory principles to ensure mono-allelic Xist upregulation, as in other unrelated molecular decision-making processes.

We have identified the simplest network that can explain the onset of random XCI. Although its mechanistic implementation might be more complex, our generic network can nevertheless serve as a framework to uncover the molecular identity of key regulators. Our approach is highly complementary to previous studies that have identified and characterized individual Xist regulators[13–15,33]. All known X-linked regulators can be grouped according to the classification that we have developed (Table 1). Autosomal factors might modulate reaction rates in a differentiation-dependent manner (for example, pluripotency factors[34–36]) or mediate the effects of X-linked regulators (for example, Rex1 as a target of RNF12 (ref. [37])), although this is not explicitly accounted for in our modeling framework. X-linked regulators outside of the identified core network might confer additional robustness (for example, *Jpx*) or mediate interactions within the core network (for example, a tXA factor could target *Ftx*).

So far, two *trans*-acting activators of Xist have been proposed (Table 1), the E3 ubiquitin ligase RNF12, which targets the Xist repressor Rex1 (Zpf42) for degradation, and the lncRNA *Jpx*[13,15,37,38]. *Jpx* escapes XCI, whereas *Rnf12* is silenced rapidly by Xist and is therefore thought to form the *trans*-acting negative feedback loop that we also identified through our network screening approach[15]. Although RNF12 overexpression can induce Xist ectopically in male cells, its deletion in females cannot prevent Xist upregulation[15,39–41]. Thus, RNF12 acts in concert with other tXA regulators, or a so far unidentified tXA factor mediates the *trans*-acting negative feedback.

The cXR factor is likely to be a lncRNA, as they frequently act *in cis*[42]. In mice, two such loci, *Tsix* and *Linx (Ppnx)* have been described[12,33]. As transcription seems to be dispensable for the function of *Linx* (R. Galupa and E.H., personal communication), it is probably insensitive to Xist-mediated silencing and would not form a double negative feedback loop. *Tsix*, by contrast, exerts its repressive function by transcription through the *Xist* promoter, where it induces repressive histone modifications[43,44]. We use a mechanistic mathematical model to show that mutual repression of *Xist* and *Tsix* can generate a local switch. Through transcriptional interference, which we confirmed experimentally, antisense transcription can generate the precise threshold required for reliable mono-allelic Xist upregulation. Although the function of *Tsix* in mice is well documented, its conservation in other mammals, such as humans, has not been shown[2]. So far, human *TSIX* has not been detected in embryonic stem cells or in embryos. Its transcription has only been reported in poorly defined embryoid body–derived cells, albeit truncated compared to mouse *Tsix* and co-expressed with *XIST* from the same allele[8]. However, since the establishment of random XCI has not yet been observed *in vivo* or *in vitro*, it might still be accompanied by *TSIX* transcription[45]. Even with the reduced overlap between *XIST* and *TSIX* reported for the human locus, the transcriptional interference-based switch assumed in our antisense model could in principle ensure mono-allelic XIST expression (Supplementary Fig. 6). The functional conservation of *TSIX* in humans therefore remains an open question.

The positive feedback loop predicted to generate bistability is not necessarily mediated by mutual repression of *Xist* and a cXR. Also, differential chromatin modifications can maintain alternative states; for example, at imprinted loci or at the *flc* locus in *Arabidopsis*[46–49]. Positive feedback loops are, for example, formed through reciprocal stimulation of CpG and H3K9 methylation or through mutual antagonism of Polycomb repression and transcription-associated H3K36 methylation[46,50].

Although the precise implementation of the positive feedback might vary between different mammals, the basic network structure that we have identified can recapitulate all expression patterns observed in mice, humans and rabbits. Depending on the relative time scales of Xist upregulation and gene silencing, the same network can recapitulate both low and high levels of bi-allelic Xist upregulation as observed in mice and rabbit embryos, respectively[3–5]. Through ectopic induction of bi-allelic Xist expression we show that this state is reversible during early differentiation. This probably also occurs in mouse embryos *in vivo*, where we observe approximately 20% bi-allelic Xist expression at the onset of random XCI, in agreement with another recent study[21].

Human pre-implantation embryos seem to be special because the silencing ability of XIST is reduced or even absent[3,6], possibly because factors that mediate silencing are not expressed at these developmental stages. The network that we have identified predicts extended bi-allelic Xist expression (as observed in human embryos[3]) to arise from reduced gene silencing if either (1) cXR was not yet expressed at this stage, or (2) cXR was dampened, while tXA was insensitive to XIST, assuming variable sensitivity to dampening across genes. Establishment of the silencing capacity of XIST (together with cXR upregulation in scenario 1) would induce a transition to the mono-allelic state. In particular, scenario 1 is intriguing because antisense transcription, which appears to function as cXR

in mice, is not observed during human pre-implantation development but could potentially be upregulated when the transition to the mono-allelic state occurs. Although so far the onset of random XCI has not been recapitulated with human ESCs[45], further refinement of the culture conditions will hopefully allow us to test whether mono-allelic XIST expression is established once silencing sets in and whether this might be accompanied by antisense transcription. Taken together, our study reveals that the regulatory principles employed by different mammalian species might be less diverse than previously thought and that the different routes to the mono-allelic state could be attributed to quantitative differences in reaction rates rather than qualitative differences in the network architecture.

Online content

Any methods, additional references, Nature Research reporting summaries, source data, statements of data availability and associated accession codes are available at https://doi.org/10.1038/s41594-019-0214-1.

Received: 15 August 2018; Accepted: 7 March 2019;
Published online: 8 April 2019

References

1. Augui, S., Nora, E. P. & Heard, E. Regulation of X-chromosome inactivation by the X-inactivation centre. *Nat. Rev. Genet.* **12**, 429–442 (2011).
2. Sado, T. & Sakaguchi, T. Species-specific differences in X chromosome inactivation in mammals. *Reproduction* **146**, R131–R139 (2013).
3. Okamoto, I. et al. Eutherian mammals use diverse strategies to initiate X-chromosome inactivation during development. *Nature* **472**, 370–374 (2011).
4. Mak, W. et al. Reactivation of the paternal X chromosome in early mouse embryos. *Science* **303**, 666–669 (2004).
5. Okamoto, I., Otte, A. P., Allis, C. D., Reinberg, D. & Heard, E. Epigenetic dynamics of imprinted X inactivation during early mouse development. *Science* **303**, 644–649 (2004).
6. Petropoulos, S. et al. Single-cell RNA-seq reveals lineage and X chromosome dynamics in human preimplantation embryos. *Cell* **165**, 1012–1026 (2016).
7. Lee, J. T. & Lu, N. Targeted mutagenesis of *Tsix* leads to nonrandom X inactivation. *Cell* **99**, 47–57 (1999).
8. Migeon, B. R., Lee, C. H., Chowdhury, A. K. & Carpenter, H. Species differences in *TSIX*/*Tsix* reveal the roles of these genes in X-chromosome inactivation. *Am. J. Hum. Genet.* **71**, 286–293 (2002).
9. Vallot, C. et al. *XACT* noncoding RNA competes with *XIST* in the control of X chromosome activity during human early development. *Cell Stem Cell* **20**, 102–111 (2017).
10. Brown, C. J. et al. The human *XIST* gene: analysis of a 17 kb inactive X-specific RNA that contains conserved repeats and is highly localized within the nucleus. *Cell* **71**, 527–542 (1992).
11. Monkhorst, K. et al. The probability to initiate X chromosome inactivation is determined by the X to autosomal ratio and X chromosome specific allelic properties. *PLoS ONE* **4**, e5616 (2009).
12. Nora, E. P. et al. Spatial partitioning of the regulatory landscape of the X-inactivation centre. *Nature* **485**, 381–385 (2012).
13. Tian, D., Sun, S. & Lee, J. T. The long noncoding RNA, Jpx, is a molecular switch for X chromosome inactivation. *Cell* **143**, 390–403 (2010).
14. Furlan, G. et al. The *Ftx* noncoding locus controls x chromosome inactivation independently of its RNA products. *Mol. Cell* **70**, 462–472.e8 (2018).
15. Jonkers, I. et al. RNF12 is an X-encoded dose-dependent activator of X chromosome inactivation. *Cell* **139**, 999–1011 (2009).
16. Monkhorst, K., Jonkers, I., Rentmeester, E., Grosveld, F. & Gribnau, J. X. Inactivation counting and choice is a stochastic process: evidence for involvement of an X-linked activator. *Cell* **132**, 410–421 (2008).
17. Sun, S. et al. Jpx RNA activates *Xist* by evicting CTCF. *Cell* **153**, 1537–1551 (2013).
18. Endo, S., Takagi, N. & Sasaki, M. The late-replicating X chromosome in digynous mouse triploid embryos. *Dev. Genet.* **3**, 165–176 (1982).
19. Henery, C. C., Bard, J. B. & Kaufman, M. H. Tetraploidy in mice, embryonic cell number, and the grain of the developmental map. *Dev. Biol.* **152**, 233–241 (1992).
20. Guyochin, A. et al. Live cell imaging of the nascent inactive X chromosome during the early differentiation process of naive ES cells towards epiblast stem cells. *PLoS ONE* **9**, e116109 (2014).
21. Sousa, E. J. et al. Exit from naive pluripotency induces a transient X chromosome inactivation-like state in males. *Cell Stem Cell* **22**, 919–928.e6 (2018).
22. Schulz, E. G. et al. The two active X chromosomes in female ESCs block exit from the pluripotent state by modulating the ESC signaling network. *Cell Stem Cell* **14**, 203–216 (2014).
23. Willard, H. F. & Carrel, L. Making sense (and antisense) of the X inactivation center. *Proc. Natl Acad. Sci. USA* **98**, 10025–10027 (2001).
24. Loos, F. et al. Xist and tsix transcription dynamics is regulated by the X-to-autosome ratio and semistable transcriptional states. *Mol. Cell. Biol.* **36**, 2656–2667 (2016).
25. Shearwin, K. E., Callen, B. P. & Egan, J. B. Transcriptional interference—a crash course. *Trends Genet.* **21**, 339–345 (2005).
26. Sneppen, K. et al. A mathematical model for transcriptional interference by RNA polymerase traffic in *Escherichia coli*. *J. Mol. Biol.* **346**, 399–409 (2005).
27. Nakanishi, H., Mitarai, N. & Sneppen, K. Dynamical analysis on gene activity in the presence of repressors and an interfering promoter. *Biophys. J.* **95**, 4228–4240 (2008).
28. Hobson, D. J., Wei, W., Steinmetz, L. M. & Svejstrup, J. Q. RNA polymerase II collision interrupts convergent transcription. *Mol. Cell* 48, 365–374 (2012).
29. Wutz, A., Rasmussen, T. P. & Jaenisch, R. Chromosomal silencing and localization are mediated by different domains of Xist RNA. *Nat. Genet.* **30**, 167–174 (2002).
30. Penny, G. D., Kay, G. F., Sheardown, S. A., Rastan, S. & Brockdorff, N. Requirement for *Xist* in X chromosome inactivation. *Nature* **379**, 131–137 (1996).
31. Lee, J. T. Regulation of X-chromosome counting by *Tsix* and *Xite* sequences. *Science* **309**, 768–771 (2005).
32. Zhou, J. X. & Huang, S. Understanding gene circuits at cell-fate branch points for rational cell reprogramming. *Trends Genet.* **27**, 55–62 (2011).
33. Lee, J. T., Davidow, L. S. & Warshawsky, D. Tsix, a gene antisense to Xist at the X-inactivation centre. *Nat. Genet.* **21**, 400–404 (1999).
34. Navarro, P. et al. Molecular coupling of *Xist* regulation and pluripotency. *Science* **321**, 1693–1695 (2008).
35. Donohoe, M. E., Silva, S. S., Pinter, S. F., Xu, N. & Lee, J. T. The pluripotency factor Oct4 interacts with Ctcf and also controls X-chromosome pairing and counting. *Nature* **460**, 128–132 (2009).
36. Schulz, E. G. & Heard, E. Role and control of X chromosome dosage in mammalian development. *Curr. Opin. Genet. Dev.* **23**, 109–115 (2013).
37. Gontan, C. et al. RNF12 initiates X-chromosome inactivation by targeting REX1 for degradation. *Nature* **485**, 386–390 (2012).
38. Gontan, C. et al. REX1 is the critical target of RNF12 in imprinted X chromosome inactivation in mice. *Nat. Comm.* **9**, 4752 (2018).
39. Barakat, T. S. et al. RNF12 activates *Xist* and is essential for X chromosome inactivation. *PLoS Genet.* **7**, e1002001 (2011).
40. Wang, F. et al. Rlim-dependent and -independent pathways for X chromosome inactivation in female ESCs. *Cell Rep.* **21**, 3691–3699 (2017).
41. Shin, J. et al. RLIM is dispensable for X-chromosome inactivation in the mouse embryonic epiblast. *Nature* **511**, 86–89 (2014).
42. Quinn, J. J. & Chang, H. Y. Unique features of long non-coding RNA biogenesis and function. *Nat. Rev. Genet.* **17**, 47–62 (2016).
43. Navarro, P., Page, D. R., Avner, P. & Rougeulle, C. *Tsix*-mediated epigenetic switch of a CTCF-flanked region of the *Xist* promoter determines the *Xist* transcription program. *Genes Dev.* **20**, 2787–2792 (2006).
44. Sado, T., Hoki, Y. & Sasaki, H. *Tsix* silences *Xist* through modification of chromatin structure. *Dev. Cell* **9**, 159–165 (2005).
45. Khan, S. A., Audergon, P. N. C. B. & Payer, B. X-chromosome activity in naive human pluripotent stem cells—are we there yet? *Stem Cell Invest.* **4**, 54–54 (2017).
46. Rose, N. R. & Klose, R. J. Understanding the relationship between DNA methylation and histone lysine methylation. *Biochim. Biophys. Acta* **1839**, 1362–1372 (2014).
47. Inoue, A., Jiang, L., Lu, F., Suzuki, T. & Zhang, Y. Maternal H3K27me3 controls DNA methylation-independent imprinting. *Nature* **547**, 419–424 (2017).
48. Angel, A., Song, J., Dean, C. & Howard, M. A Polycomb-based switch underlying quantitative epigenetic memory. *Nature* **476**, 105–108 (2011).
49. Dodd, I. B., Micheelsen, M. A., Sneppen, K. & Thon, G. Theoretical analysis of epigenetic cell memory by nucleosome modification. *Cell* **129**, 813–822 (2007).
50. Yang, H., Howard, M. & Dean, C. Antagonistic roles for H3K36me3 and H3K27me3 in the cold-induced epigenetic switch at arabidopsis FLC. *Curr. Biol.* **24**, 1793–1797 (2014).
51. Sakata, Y. et al. Defects in dosage compensation impact global gene regulation in the mouse trophoblast. *Development* **144**, 2784–2797 (2017).
52. Barakat, T. S. et al. The trans-activator RNF12 and cis-acting elements effectuate X chromosome inactivation independent of X-pairing. *Mol. Cell* **53**, 965–978 (2014).

Acknowledgements

We thank A. Wutz (ETH Zürich, Switzerland) for the TXY (Xist-tetOP) and TXYΔA (Xist-ΔSX-tetOP) mESC lines. We thank the staff of the Max Planck Institute for Molecular Genetics (MPIMG) and PICTIBiSA@BDD imaging facilities for technical

assistance, the MPIMG sequencing core facility of sequencing services and the MPIMG IT facility for support in using the computing cluster. We thank R. Galupa for valuable feedback on the manuscript. This work was funded by a Human Frontier Science Program (HFSP) long-term fellowship (LT000597/2010-L) to E.G.S., a Grant-in-Aid for Specially Promoted Research from the Japan Society for the Promotion of Science (JSPS) (17H06098) to M.S., and by a Japan Science and Technology Agency (JST) Exploratory Research for Advanced Technology (ERATO) grant (JPMJER1104) to M.S., I.O. and M.S., and JSPS KAKENHI grants (25291076 and 18K06030) to I.O. Reseach in the laboratory of E.G.S. is funded by the Max-Planck Research Group Leader program and and the German Ministry of Science and Education (BMBF) through the grant E:bio Module III - Xnet. V.M. is supported by the DFG (GRK1772, Computational Systems Biology). Research in the laboratory of L.G. is funded by an ERC Starting grant (759366).

Author contributions

E.G.S., E.H. and I.O. conceived the study. V.M. and E.G.S. wrote scripts and performed simulations. V.M., I.O., I.D., L.G. and E.G.S. carried out the experiments. E.G.S. and V.M. wrote the paper with input from E.H. and L.G. E.G.S., E.H. and M.S. supervised the study. E.G.S., E.H., L.G., I.O. and M.S. acquired funding.

Competing interests

The authors declare no competing interests.

Additional information

Supplementary information is available for this paper at https://doi.org/10.1038/s41594-019-0214-1.

Reprints and permissions information is available at www.nature.com/reprints.

Correspondence and requests for materials should be addressed to E.G.S.

Methods

ODE simulations. ODE models were formulated by assuming a Hill type regulation of production rates and first-order degradation rates, such that the levels of all variables were scaled between 0 and 1. Interaction between two regulators was assumed to occur synergistically, such that their effects are multiplied. The equation systems were simulated in MATLAB_R2016b using the ode23tb integrator for 100 h, and the final state was used to solve for the steady state using the function fsolve. Details are given in Supplementary Note 1.

Stochastic simulations of the cXR–tXA model. Reactions describing production and degradation reactions were formulated directly from the ODE model, by adding scaling factors that would determine the maximal number of molecules that can be produced for a given variable. Moreover, each Xist molecule had to transition through a certain number of silencing intermediates (with rate 1 h^{-1}) before reaching a silencing-competent state. The silencing delay for cXR (sil_{cXR}) and tXA (sil_{cXR}) was then given by the number of required silencing intermediates and is equal to the mean silencing delay. The simulations were performed using the Gillespie algorithm[53], implemented in Julia_v0.6 and executed on a computing cluster. To identify parameter sets that could reproduce the experimental data, a large number of randomly chosen parameter sets were simulated. Experimental data and simulations were modeled with a multinomial distribution and a maximum likelihood estimate (MLE) was used to identify the parameter set that best explained the data. For further details, see Supplementary Note 2.

Stochastic simulations of the antisense model. To simulate antisense transcription, RNA Pol II molecules were assumed to bind to the promoters of *Tsix* and *Xist* in a stochastic fashion and then move deterministically along the respective gene, which had been divided into 100 nt-long segments. For elongation and degradation rates, experimental estimates from the literature were used[54–56]. When Xist RNA exceeds a threshold of 10 molecules, the *Tsix* promoter will switch to the OFF state with the silencing delay sil_{Tsix}. Transcription of a *Tsix* polymerase through the *Xist* promoter induced a switch to the OFF state that could revert back to the ON state with a constant rate. When two RNA Pol II molecules occupied the same DNA segment, one randomly chosen polymerase was removed from the gene. The tXA produced per allele was scaled between 0 and 1 and was set to 0 with a certain delay after Xist had exceeded a threshold of 10 molecules. Simulations were conducted in MATLAB_R2014b. The model was written in C++ and compiled into a MEX file that was called from the main MATLAB function. For parameter scanning, a compiled MATLAB script was executed in parallel on a computing cluster.

Cell lines. The female TX1072 cell line and its subclone TX1072 XO (clone A11) are F1 hybrid ESCs (CastxB6), which carry a doxycycline responsive promoter in front of the *Xist* gene on the B6 chromosome and an rtTA (reverse tetracycline-controlled transactivator) insertion in the Rosa26 locus (described in ref. [22]). The TX1072dT line (clone 1C6) was generated by introducing a deletion of the Dxpas34 repeat in TX1072 cells on the Cast chromosome by co-transfecting Cas9 expression vectors p330 (ref. [57]) expressing sgRNAs GTACATAATGACCCGATCTC and GA ACTCACTATATCGCCAAAG. pX330 was a gift from Feng Zhang. Clones with the deletion were identified by PCR (ES585, AGGCACACCACCCCAGTGGA;ES609, TCCAAACATGGCGGCAGAAGC) and the deleted allele was identified by Sanger sequencing of the PCR product using primer ES609 based on two SNPs at positions 100,645,601 (Cast, C) and 100,641,221 (Cast, G) (mm9). Male-inducible wild-type and ΔA *Xist* lines were a gift from A. Wutz (called *Xist*-tetOP and *Xist*-ΔSX-tetOP, respectively, in ref. [29]). All cell lines were regularly confirmed to be mycoplasma-negative.

ESC culture and differentiation. TX1072, TX1072XO and TX1072dT cells were grown on gelatin-coated flasks in serum-containing ESC medium (DMEM (Sigma), 15% FBS (Gibco), 0.1 mM β-mercaptoethanol, 1,000 U ml^{-1} leukemia inhibitory factor (LIF, Millipore)), supplemented with 2i (3 μM Gsk3 inhibitor CT-99021, 1 μM MEK inhibitor PD0325901) for TX1072 and TX1072 XO. Differentiation was induced by 2i/LIF withdrawal in DMEM supplemented with 10% FBS and 0.1 mM β-mercaptoethanol at a density of 4×10^4cells cm^{-2} in fibronectin (10 μg ml^{-1}) coated tissue culture plates. For ectopic Xist induction, the medium was supplemented with 1 μg ml^{-1} doxycycline. To induce Xist in undifferentiated cells, they were plated at a density of 1×10^5cells cm^{-2} 2 d before collection and treated with 1 μg ml^{-1} doxycycline. Male-inducible wild-type and ΔA *Xist* lines were plated at a density of 3×10^4cells cm^{-2} on mitomycin C-inactivated mouse embryonic fibroblasts in ESC media containing 15% FBS (Gibco), 0.1 mM β-mercaptoethanol (Sigma), 1,000 U ml^{-1} LIF (Millipore) and treated for 24 h with 2 μg ml^{-1} doxycycline 1 d after plating.

Mice. All animal experiments were performed in accordance with the ethical guidelines for the Care and Use of Laboratory Animals (French Ethical Committee on Animal Experimentation, Institut Curie 118; and agreement C75-05-17 of the animal facility of Kyoto University). Embryos were obtained by natural mating between B6D2F1 (derived from C57BL/6J and DBA2 crosses) female and males. Noon of the day when vaginal plugs were detected was set as E0.5.

Conventional RNA FISH on ESCs. FISH on cells from tissue culture was performed as described previously[58]. In brief, mESCs were dissociated using Accutase (Invitrogen) and adsorbed onto coverslips (#1.5, 1 mm) coated with Poly-L-Lysine (Sigma) for 5 min. Cells were fixed with 3% paraformaldehyde in PBS for 10 min at room temperature (18–24 °C) and permeabilized for 5 min on ice in PBS containing 0.5%Triton X-100 and 2 mM Ribonucleoside Vanadyl complex (New England Biolabs). Coverslips were preserved in 70% EtOH at -20°C. Prior to FISH, samples were dehydrated through an ethanol series (80%, 95%, 100% twice) and air-dried for 1–3 min until no more ethanol was visible. To detect the X-linked transcript Huwe1 (to verify the presence of two X chromosomes), a BAC (bacterial artificial chromosome) spanning the respective genomic region (RP24-157H12) was labeled by nick translation (Abbot) using dUTP-Atto550 (Jena Bioscience). Per coverslip, 60 ng probe was ethanol precipitated with Cot1 repeats, resuspended in formamide, denatured (10 min 75°C) and competed for 1 h at 37 °C. Xist was detected with a custom-designed strand-specific probe that densely tiles all exons with approximately 75-bp-long oligonucleotides end-labeled with the Alexa488 fluorophore (Roche). Both probes were co-hybridized in FISH hybrization buffer (50% formamide, 20% dextran sulfate, 2× SSC, 1 μg $μl^{-1}$ BSA, 10 mM vanadyl ribonucleoside) overnight. Washes were carried out at 42 °C three times for 7 min in 50% formamide in 2× SSC at pH 7.2 and three times for 5 min in 2× SSC. DAPI (4′,6-diamidino-2-phenylindole; 0.2 mg ml^{-1}) was used for counterstaining, and mounting medium consisted of 90% glycerol, 0.1× PBS, 0.1% p-phenylenediamine at pH 9 (Sigma). Images were acquired using a wide-field DeltaVision Core microscope (Applied Precision) or a widefield Z1 Observer (Zeiss) using a ×100 objective.

Immunofluorescence combined with RNA FISH. For immunofluorescence staining, cells were differentiated on fibronectin coated cover slips (18 mm, Marienfeld) at a density of 2×10^4cells cm^{-2}. Cells were fixed and permeabilized as described above and incubated with the H3K27me3 antibody (Active Motif 39155, 0.4 μg ml^{-1}) in PBS for 1 h at room temperature, then washed three times for 10 min with PBS, followed by a 1 h incubation with an Alexa-555 labelled Goat anti-rabbit antibody (Invitrogen A-21428, 0.8 μg ml^{-1}). After three washes, the cells were fixed again with 3% paraformaldehyde in PBS for 10 min at room temperature, followed by three short washes with PBS and two washes with SSC. Hybridization was then performed as described above. Details on the antibodies used are found in supplementary Table 1.

EdU staining combined with RNA FISH. Cells were differentiated on fibronectin-coated cover slips (18 mm, Marienfeld) at a density of 2×10^4cells cm^{-2} and were treated with 7.5 μM EdU (Component A from Click-iT EdU Imaging kit Invitrogen C10340) for 2 h before collection. Cells were fixed and permeabilized as described above, except that fixation and permeabilization were carried out at room temperature for 15 and 20 min, respectively. EdU staining with Alexa Fluor 647 was performed according to the manufacturer's recommendations, followed by RNA FISH for Xist as described above.

Quantitative RNA FISH. Quantitative RNA FISH on Xist and Tsix was performed using Stellaris FISH probes (Biosearch Technologies). Probe details can be found in Supplementary Table 1. Cells were adsorbed and fixed as described above. Cells were prehybridized in wash buffer (2× SSC, 10% formamide) twice for 5 min, then hybridized with a solution that contained 125 nM of each FISH probe, 2× SSC, 10% formamide, 10% dextran sulfate overnight at 37 °C. Cells were washed twice with wash buffer for 30 min before counterstaining DNA with 0.2 mg ml^{-1} DAPI in 1× PBS, and mounted on slides using the mounting medium described above. Z-stacks were acquired using a wide-field Z1 observer (Zeiss) microscope equipped with a ×100 objective (voxel size 88 × 88 × 200 nm). Quantification of nascent RNA signals was performed as in ref. [59]. In brief, the fluorescence background of each *z* plane was generated by morphologically opening the image with a circular structuring element with a diameter of 5 pixels (440 nm), and subtracted from the original image. A region of interest (ROI) of constant volume (30 × 30 × 6 pixels = 2.6 × 2.6 × 1.2 μm) was selected around each transcription site. To reduce residual high-frequency fluorescence background, the average pixel intensity was measured in a 3-voxel-thick frame adjacent to the border of the ROI, and further subtracted. The integrated intensity of the fluorescent signal was then measured within the whole ROI. Integrated intensities of approximately 500 random nuclear background ROIs were used to define a threshold (mean + 5 s.d. after removing top 1% as outliers) to classify transcribed versus non transcribed loci.

RNA FISH of epiblast cells from E5.0 embryos. E5.0 mouse embryos were dissected out from the decidua and the Reichert's membrane was removed in a 6 cm Petri dish containing PBS using sharpened forceps. Extra-embryonic ectoderm was separated using a fine glass needle. The epiblast and visceral endoderm were incubated in 0.25% pancreatin (Sigma), 0.5% trypsin and polyvinylpyrrolidone (PVP40, Sigma) at 4 °C for 10 min and transferred to a 3.5 cm petri dish containing a large volume of 1% BSA in PBS. Epiblast and visceral endoderm were separated using a mouth pipette with an internal diameter slightly smaller than that of the epiblast. RNA FISH was carried out as described previously[5], using a non-strand-specific probe detecting Xist and Tsix (p510). Embryos with a Xist cloud were identified as female. Images were acquired using a 200 M Axiovert fluorescence microscope (Zeiss) equipped with an ApoTome

to generate 3D optical sections. Sequential *z*-axis images were collected in 0.3 µm steps. Images were analyzed using ImageJ software (Fiji, NIH).

RNA extraction, reverse transcription, qPCR. For pyrosequencing and quanitative PCR (qPCR), cells were lysed by direct addition of 1 ml Trizol (Invitrogen). Then 200 µl of chloroform was added and after 15 min centrifugation (12,000 × *g*, 4 °C) the aqueous phase was mixed with 700 µl 70% ethanol and applied to a Silica column (Qiagen RNAeasy Mini kit). RNA was then purified according to the manufacturer's recommendations, including on-column DNAse digestion. For qPCR, 1 µg RNA was reverse transcribed using a Superscript III Reverse Transcriptase (Invitrogen). Expression levels were quantified using 2× SybRGreen Master Mix (Applied Biosystems) and a ViiA7 system (Applied Biosystems) with approximately 8 ng cDNA and the primers given in Supplementary Table 1. Expression levels were normalized to Rrm2 and Rplp0.

Allele-specific amplicon sequencing. RNA was extracted using the Direct-zol RNA MiniPrep kit (Zymo Research) and DNase digest was performed using a Turbo DNA free kit (Ambion). The TruSeq Targeted RNA Expression assay (Illumina) was used according to the manufacturer's recommendations and the samples were sequenced on a HiSeq2500. For the quantification of reference genes (Rrm2, Rplp0, Fbxo28, Exoc1) 50bp reads were aligned to the mouse reference genome (mm10) allowing two mismatches using the STAR aligner[60], and the reads covering each amplicon were counted with Bedtools multicov[61]. For allele-specific quantification, reads were aligned to either the B6 (reference) or Cast genomes with no mismatches and reads covering the SNPs were counted with Bedtool multicov. Reads for four amplicons within *Xist* exons containing SNPs were normalized to the geometric mean of the reference genes. The fold change of the doxycycline treated sample relative to the corresponding control sample was then calculated for each *Xist* amplicon. We then tested to see whether the mean $\log_2$ fold change of the four amplicons was significantly different from 0 ($P < 0.05$) using a one-sample *t*-test. Details on the amplicons are given in Supplementary Table 1.

Pyrosequencing. For allele-specific expression analysis of Tsix, pyrosequencing technology was used. Two different amplicons within Tsix, each containing a SNP, were PCR-amplified from cDNA with biotinylated primers and sequenced using the Pyromark Q24 system (Qiagen). Primer sequences are given in Supplementary Table 1. The assay provides the fraction of *Tsix* transcript arising from the B6 chromosome at time *t* (F_t). To calculate the expression from the B6 chromosome at time *t* relative to the uninduced state at $t = 0$ h $\left(\frac{B6_t}{B6_0}\right)$, the data were transformed as follows. Assuming that expression from the Cast chromosome is constant over time, $F_0 = \frac{B6_0}{B6_0 + Cast}$ and $F_t = \frac{B6_t}{B6_t + Cast}$ can be transformed into $\frac{B6_t}{B6_0} = \frac{F_t(1 - F_0)}{F_0(1 - F_t)}$.

Statistics. Statistical significance was evaluated using a two-sided one- or two-sample *t*-test, as indicated in the figure legends.

Reporting Summary. Further information on research design is available in the Nature Research Reporting Summary linked to this article.

Data availability

Source data for Figs. 3c,d, 4b,c,f,g,i, 5d and 6c–f and Supplementary Figs. 1 and 3a,b,d are available with the paper online. Data, code and simulations used in this study are available at https://github.com/verenamutzel/XCI_model under the MIT license. All other data and the cell line TX1072dT generated for this study are available upon reasonable request.

Code availability

All code and simulations used in this study are available at https://github.com/verenamutzel/XCI_model under the MIT license.

References

53. Gillespie, D. T. Exact stochastic simulation of coupled chemical reactions. *J. Phys. Chem.* **81**, 2340–2361 (1977).
54. Jonkers, I., Kwak, H., Lis, J. T. & Struhl, K. Genome-wide dynamics of Pol II elongation and its interplay with promoter proximal pausing, chromatin, and exons. *eLife* **3**, e02407 (2014).
55. Sun, B. K., Deaton, A. M. & Lee, J. T. A transient heterochromatic state in *Xist* preempts X inactivation choice without RNA stabilization. *Mol. Cell* **21**, 617–628 (2006).
56. Yamada, N. et al. Xist exon 7 contributes to the stable localization of *Xist* RNA on the inactive X-chromosome. *PLoS Genet.* **11**, e1005430 (2015).
57. Ran, F. A. et al. Genome engineering using the CRISPR-Cas9 system. *Nat. Protoc.* **8**, 2281–2308 (2013).
58. Chaumeil, J., Augui, S., Chow, J. C. & Heard, E. Combined immunofluorescence, RNA fluorescent in situ hybridization, and DNA fluorescent in situ hybridization to study chromatin changes, transcriptional activity, nuclear organization, and X-chromosome inactivation. *Methods Mol. Biol.* **463**, 297–308 (2008).
59. Giorgetti, L. et al. Predictive polymer modeling reveals coupled fluctuations in chromosome conformation and transcription. *Cell* **157**, 950–963 (2014).
60. Dobin, A. et al. STAR: ultrafast universal RNA-seq aligner. *Bioinformatics* **29**, 15–21 (2012).
61. Quinlan, A. R. & Hall, I. M. BEDTools: a flexible suite of utilities for comparing genomic features. *Bioinformatics* **26**, 841–842 (2010).

nature research

Corresponding author(s): Edda G. Schulz

Reporting Summary

Nature Research wishes to improve the reproducibility of the work that we publish. This form provides structure for consistency and transparency in reporting. For further information on Nature Research policies, see Authors & Referees and the Editorial Policy Checklist.

Statistical parameters

When statistical analyses are reported, confirm that the following items are present in the relevant location (e.g. figure legend, table legend, main text, or Methods section).

n/a	Confirmed	
☐	☒	The exact sample size (*n*) for each experimental group/condition, given as a discrete number and unit of measurement
☐	☒	An indication of whether measurements were taken from distinct samples or whether the same sample was measured repeatedly
☐	☒	The statistical test(s) used AND whether they are one- or two-sided *Only common tests should be described solely by name; describe more complex techniques in the Methods section.*
☒	☐	A description of all covariates tested
☒	☐	A description of any assumptions or corrections, such as tests of normality and adjustment for multiple comparisons
☐	☒	A full description of the statistics including central tendency (e.g. means) or other basic estimates (e.g. regression coefficient) AND variation (e.g. standard deviation) or associated estimates of uncertainty (e.g. confidence intervals)
☐	☒	For null hypothesis testing, the test statistic (e.g. *F*, *t*, *r*) with confidence intervals, effect sizes, degrees of freedom and *P* value noted *Give P values as exact values whenever suitable.*
☒	☐	For Bayesian analysis, information on the choice of priors and Markov chain Monte Carlo settings
☒	☐	For hierarchical and complex designs, identification of the appropriate level for tests and full reporting of outcomes
☒	☐	Estimates of effect sizes (e.g. Cohen's *d*, Pearson's *r*), indicating how they were calculated
☐	☒	Clearly defined error bars *State explicitly what error bars represent (e.g. SD, SE, CI)*

Our web collection on statistics for biologists may be useful.

Software and code

Policy information about availability of computer code

Data collection	Zen software (Zeiss) was used for image aquisition.
Data analysis	For simulations custom scripts were written in Matlab, C++ and Julia. For image analysis a macro programmed in ImageJ was used.

For manuscripts utilizing custom algorithms or software that are central to the research but not yet described in published literature, software must be made available to editors/reviewers upon request. We strongly encourage code deposition in a community repository (e.g. GitHub). See the Nature Research guidelines for submitting code & software for further information.

Data

Policy information about availability of data

All manuscripts must include a data availability statement. This statement should provide the following information, where applicable:

- Accession codes, unique identifiers, or web links for publicly available datasets
- A list of figures that have associated raw data
- A description of any restrictions on data availability

All data, code and simulations used in this study are available at https://github.com/verenamutzel/XCI_model under the MIT license. Source data for figure 3c, 3d, 4b, 4c, 4f, 4g, 4i, 5d, 6c-f, S1, S3a, S3b, S3d are available with the paper online. The cell line TX1072dT generated for this study is available upon request.

Field-specific reporting

Please select the best fit for your research. If you are not sure, read the appropriate sections before making your selection.

☒ Life sciences ☐ Behavioural & social sciences ☐ Ecological, evolutionary & environmental sciences

For a reference copy of the document with all sections, see nature.com/authors/policies/ReportingSummary-flat.pdf

Life sciences study design

All studies must disclose on these points even when the disclosure is negative.

Sample size	All experiments were performed in triplicate to assess whether the observed effects were reproducible. For the in vivo analysis 15 embryos were analyzed, all of which showed the same effect (10-20% of bi-allelic Xist expression).
Data exclusions	no data was excluded.
Replication	All observations were replicated at least 3 times.
Randomization	No randomization was included in the study design.
Blinding	Blinding was not possible, since a single person acquired and analysed the data.

Reporting for specific materials, systems and methods

Materials & experimental systems

n/a	Involved in the study
☐	☒ Unique biological materials
☐	☒ Antibodies
☐	☒ Eukaryotic cell lines
☒	☐ Palaeontology
☐	☒ Animals and other organisms
☒	☐ Human research participants

Methods

n/a	Involved in the study
☒	☐ ChIP-seq
☒	☐ Flow cytometry
☒	☐ MRI-based neuroimaging

Unique biological materials

Policy information about availability of materials

Obtaining unique materials	The cell line TX1072dT generated for this study is available upon request.

Antibodies

Antibodies used	H3K27me3 antibody: Active Motif #39155, 0.4ug/ml
Validation	The antibody staining co-localizes as expected with Xist at the inactive X-chromosome

Eukaryotic cell lines

Policy information about cell lines

Cell line source(s)	Male-inducible wild-type and ΔA Xist lines were a gift from A. Wutz. The female TX1072 cell line and its subclone TX1072 XO (clone A11) were previously derived in Edith Heard's lab by Edda Schulz (Schulz et al, Cell Stem Cell, 2014).
Authentication	The number of X chromosomes was regularly checked by RNA FISH for X-linked genes. All cell lines used carry an inducible Xist promoter. Xist induction by doxycyline treatment was verified by RNA FISH and/or qPCR.
Mycoplasma contamination	Cells were regularly tested for mycoplasma contamination, test results were always negative.

Commonly misidentified lines (See ICLAC register)	No such cell lines were used in this study.

Animals and other organisms

Policy information about studies involving animals; ARRIVE guidelines recommended for reporting animal research

Laboratory animals	Mouse embryos were obtained by natural mating between B6D2F1 (derived from C57BL/6J and DBA2 crosses) female and males.
Wild animals	No wild animals were used in this study.
Field-collected samples	No field-collected samples were used in this study.